Microstructural Characteristics of Laser-Clad AISI P20 Tool Steel

Chen, Jianyin; Xue, Lijue

Publisher's version / Version de l'éditeur:

Surface Engineering Coatings and Heat Treatments 2002, pp. 198-205, 2003-01-01

NRC Publications Record / Notice d'Archives des publications de CNRC:
https://nrc-publications.canada.ca/eng/view/object/?id=49f64de6-0052-42eb-a0f8-4eb4665c778a
https://publications-cnrc.canada.ca/fra/voir/objet/?id=49f64de6-0052-42eb-a0f8-4eb4665c778a

Submitted to 13th IFHTSE/ASM Surface Engineering Congress, 7-10 October, 2002, Columbus, Ohio, USA

Microstructural Characteristics of Laser-Clad AISI P20 Tool Steel

J.-Y. Chen and L. Xue
Integrated Manufacturing Technologies Institute
National Research Council Canada
800 Collip Circle, London, Ontario N6G 4X8, Canada

ABSTRACT

Laser cladding of P20 powder on AISI P20 tool steel substrate has been investigated for potential mold or die repair applications. The process was conducted using a 3 kW CO_2 laser in continuous wave (CW) mode to melt the moving substrate while P20 powder was simultaneously fed into the molten pool. The process can accurately deposit material at desired locations with a relatively low heat input. A dense and crack-free clad layer was obtained with an excellent metallurgical bonding with the substrate. This study demonstrates that P20 powder can be deposited on P20 tool steel substrate without any pre-heating. The P20 clad layer has a higher hardness as compared to the P20 substrate. The microstructural morphology of as-clad P20 shows predominant martensite phase along with refined dendrites due to process-induced fast cooling. Moreover, the residual stress measurements indicate the presence of compressive residual stresses on the surface of the P20 clad.

Keyword: laser cladding, P20 tool steel, microstructure

INTRODUCTION

The laser cladding process deposits a desired material onto the surface of an existing component with an excellent metallurgical bond at the interface. The process can accurately deposit material at desired locations with a relatively low heat input and dilution, and produces a refined microstructure with a better chemical homogeneity due to the inherent fast cooling induced by the process[1-3]. These features are normally not available by other conventional processes such as thermal spraying or welding. Laser cladding has been used to improve corrosion, wear, and oxidation resistance of components: for example, laser cladding of vanadium carbide on AISI H13 tool steel to improve its tribological behavior[4]; laser cladding of 304L stainless steel on the surface of plain carbon steel to improve its corrosion resistance[5]. Recently, laser cladding has been applied for repairing expensive damaged parts. For example, laser cladding of Ni-Al bronze was used to repair marine components[6]; laser cladding of superalloy was used to repair damaged engine components[7]. The repair of damaged components for subsequent reuse can substantially reduce their through-life cost.

In this paper, the results of laser cladding of P20 powder on a substrate of wrought P20 steel are presented. The P20 material is a low carbon mold steel that is commonly used for making plastic injection and some die-casting molds and dies. After a long period of service, the wear damage of molds or dies is inevitable, and consequently an adequate repair is required, particularly for expensive molds and dies. There are several possible approaches to repair these damaged modes or dies, such as, welding or cladding. In comparison with the conventional welding or thermal spraying techniques, the laser cladding has many unique advantages. For example, it could be applied on a localized area with a controllable heat input, which, in turn, leads to a significantly small heat affected zone (HAZ) and low dilution into the base material, and hence reduces minimal degradation to the base material. Furthermore, the nature of the bonding between the clad and substrate is metallurgical, thereby eliminating the possibility of debonding or peeling during service.

The objective of this paper is to document the microstructural characteristics of the laser-clad P20 tool steel as studied by Optical Microscopy (OM), Scanning Electron Microscopy (SEM) and X-Ray Diffraction (XRD) techniques. The nature and magnitude of the process-induced residual stresses were measured and the preliminary results were also reported.

EXPERIMENTS

Material

The spherical P20 powder manufactured by Carpenter Powder Products Inc., was used as the laser cladding material with the particle size ranging from 44 to 63 μm (-230 mesh/+325 mesh). Figure 1 shows a SEM photo of the P20 powder, exhibiting that the shape of the powder was primarily spherical. Wrought P20 tool steel plates with the thickness of 12.5 mm were used as substrates. The chemical compositions of P20 powder and P20 tool steel substrate are shown in Table 1. Prior to any laser cladding, all P20 substrates were ground to maintain a consistent surface finish and degreased with acetone.

Table 1: The chemical compositions of P20 powder and P20 tool steel substrate (wt%)

Type	C	Mn	Si	S	P	Cr	Cu	Mo	Fe
Powder[8]	0.40	0.83	0.67	0.01	0.01	1.86	0.02	0.53	Balance
Substrate[9]	0.28-0.40	0.60-1.00	0.20-0.80	-	-	1.40-2.00	-	0.30-0.55	Balance

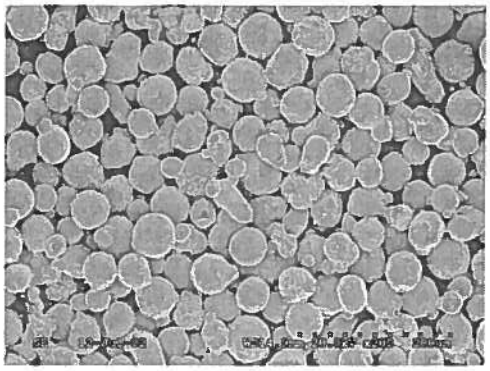

200x

Figure 1: SEM photo of P20 powder supplied by Carpenter Powder Products Inc.

Process

A blown powder laser cladding technique was used in the current investigation. In the process setup, P20 substrate was clamped on a CNC-controlled X-Y motion table. A 3 kW continuous wave (CW) CO_2 laser (GE Fanuc C3000) and a Mark XV-RC powder feeder were used in this study. The laser beam was directed, using reflecting mirrors, so that it entered the focusing optics perpendicularly. The focusing optics and the powder delivery tube were mounted on the Z-axis of the motion system. During the cladding, the laser beam and powder delivery tube were stationary while the motion table was moved at a traverse speed ranging from 5 to 12 mm/s. The laser cladding process was performed in a glove box, in which argon was used to transport the powder and to provide shielding against oxidation. The laser beam was focused on the P20 substrate by using a 190 mm focal length lens to create a molten pool, into which the P20 powder was simultaneously injected. The power density of the related laser beam was about (6~9) x 10^4 W/cm^2 while the powder feedrate was about 10-15 g/min. The focused laser beam scanned the surface of the substrate through a relative movement of the motion table to form a single cladding pass. Through subsequent overlapping passes, a thick clad layer around 2 mm in thickness was obtained after 4 layers were deposited. During the cladding the substrate temperature could increase if the size of the substrate is small and higher power density is used.

In general, process-induced residual stresses could be accumulated with an increase in the clad thickness. Particularly for tool steels, a hardened substrate is normally sensitive to the accumulated residual tensile stresses which may eventually induce cracking. For the P20 tool steel used for mold or die applications, the working hardness is around Rc. 36-38[10] prior to carburizing. In order to assess the cracking-tendency of in-service P20 tool steel during laser cladding process, all P20 substrates were heat treated before the cladding. The heat treatment procedure consisted of a heating and quenching (austenitized at 845°C and quenched in water) with subsequent tempering (205°C for 120 min). The treatment resulted in an average hardness of about Rc. 49. It should be noted that the water quenching resulted in a much higher hardness compared to oil quenching (about Rc. 36-38[10]). Generally, P20 steel is oil quenched, however, as the proper quenching oil was not available, the substrates were water quenched for the current experiments.

Characterization

After the laser cladding, all specimens were mechanically sectioned, and polished on Buehler TEXMET 2000 cloth for the metallographic study. An OLYMPUS PMG 3 Optical Microscope (OM) was used for optical microstructure observation while a Hitachi S-3500 Scanning Electron Microscope (SEM) coupled with Energy Dispersive Spectrometer (EDS) was used for high-resolution microstructure study and chemical composition analyses. In order to reveal the microstructure, the polished specimens were etched by swabbing them for approximately 35-40s with 2% nital solution. The phase identification was performed on the ground surface of clad specimens with a Philips X'Pert X-Ray Diffractometer (XRD) using Cu K_α radiation operated at 40 kV and 45 mA.

The microhardness measurements were carried out on a Buehler Micromet II Micro Hardness Tester using a Vickers indentor with 100g normal load applied for 15 s, while the overall hardness measurements were performed on a NewAge Industries ME-2 series Rockwell Hardness Testing System. Measurements were performed within the clad layer, heat affected zone (HAZ), and substrate material.

The residual stresses in the laser-clad P20 specimens were assessed using a hole-drilling strain-gauge technique. The test was conducted as per ASTM E837-95 by using an RS-200 Milling Guide manufactured by Measurement Group Inc. A special strain gage rosette (TEA-06-062RK-120) was bonded at the point of the laser-clad P20 specimen where residual stresses were to be measured. A high-speed air turbine with a carbide

cutter of 1.6 mm diameter was used to drill a hole at the centre of the rosette, while the relaxed strains around the hole were measured with the rosette and recorded by a data acquisition system. The residual stresses were then deduced through ReStress® software supplied with the system. It should be pointed out that such measured stresses reflect the local average values across a depth of 0.4 to 0.6 mm, depending on the diameter of drilled holes.

RESULTS AND DISCUSSION

Observation of Laser Clad P20 Specimens

In order to obtain a metallurgically sound and fully dense P20 clad, the processing parameters for the laser cladding were optimized by varying powder feedrate and traverse speed of the substrate while keeping the laser power and focal distance unchanged. Figure 2 shows two representative laser-clad P20 specimens with a clad thickness of about 2 mm. No cracking was observed in the P20 clad although the substrate has been heat-treated to have a hardness as high as Rc. 49, which indicates that the laser cladding can be performed on the hardened P20 substrate without the need of preheating. The penetration depth of the clad, defined as the depth of melting into the substrate, was an average of about 264 μm under the current process parameters, which is significantly lower compared to welding process which produces penetration depths in a range of millimeters.

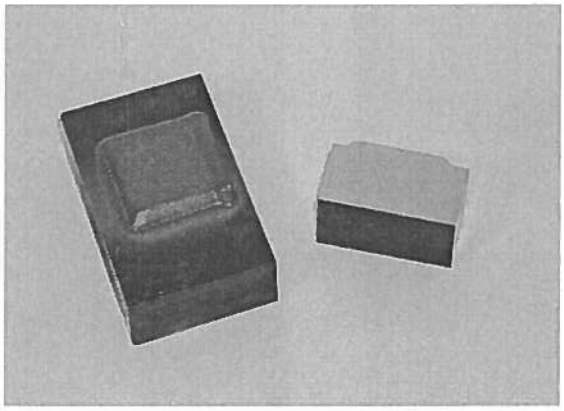

Figure 2: Laser-clad P20 specimens

The cross-section of the as-clad P20 specimen can be divided into three major regions: P20 clad layer, heat affected zone (HAZ) which was just beneath the clad layer and the P20 substrate, as shown in Figure 3. Since the laser cladding was performed using overlapping passes to cover the desired surface, any subsequent pass would always re-melt a portion of the previous pass; therefore, two types of areas can be observed within the clad layer: "as-deposited" zone and "re-melted" zone. However, the microstructural distinction between "as-deposited" and "re-melted" in this particular case was not significant because multiple self-tempering during the thickness accumulation of laser cladding (2mm thick with 4 layers) has lessened such a difference.

Figure 3: Cross-section of as-clad P20

XRD Phase Identification

X-ray diffraction analyses for both powder and as-clad P20 specimens indicate that their main phases in the specimens consisted of a predominant b.c.c. (or b.c.t.) phase and a small amount of f.c.c. austenite, as displayed in Figure 4. Nevertheless, any lines diffracted by carbides cannot be observed within the associated limits of resolution because of their low quality and low sensitivity to X-ray diffraction. As a reference, the pattern for the heat-treated P20 substrate was also measured, which indicates the presence of predominant α' martensite with no traceable γ austenite. For the P20 powder, the referred b.c.c (or b.c.t.) phase could be α' martensite or a combination of δ ferrite and α' martensite, depending on the actual cooling rate because a high cooling rate could in certain degree depress the transformation of δ ferrite into γ austenite while a relatively slow cooling rate favored the γ austenite formation, which then transformed into α' martensite[11]. The information from X-ray diffraction alone may not sufficient to identify these phases. The optical and SEM analyses would be helpful to provide additional information on the phase identification. Moreover, it has been found from the XRD patterns that

unlike most of laser consolidated alloys, there was no presence of significant preferred orientation in the P20 clad since the ratios of the relative intensity of diffracted lines for the P20 powder, P20 clad and P20 substrate did not exhibit any substantial difference.

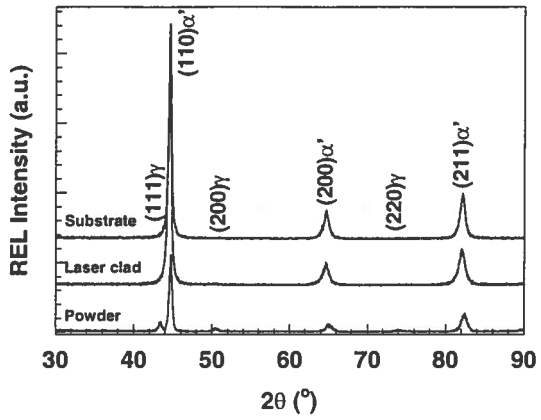

Figure 4: X-ray diffraction patterns of P20 powder, P20 clad and P20 substrate

Microstructural Characterization

As compared to the conventional welding technique, relatively fast cooling inherent to laser cladding process could produce unique microstructure with finer grain size, lower chemical segregation, stable and metastable phases, which might improve mechanical properties and hence the performance of the components. Figure 5(a) exhibits a typical SEM micrograph of as-clad P20 cross-section, where the morphology of the P20 clad was characterized by a refined dendritic structure with the first dendritic arm spacing (DAS) of around 15 to 20 μm. This is indicative of a fast cooling rate during the solidification. However, the subsequent cooling rate for the solid-state phase transformation might not be as high as expected, but still high enough to form predominantly martensite. In addition to the presence of a large amount of lath martensite, a small amount of lenticular lower bainite was also observed (see arrow in Figure 5(b)), indicating a decreased cooling rate. The reduce cooling rate could be attributed to the reduced efficiency of heat removal by a small size of substrate.

It is interesting to note that the length of lath martensite in laser-clad P20 was very short and mainly determined by the dendrite arm size. The SEM observation reveals that the lath martensite grew in "parallel" along certain orientation inside each dendrite arm until they met each other (see Figure 5(c)). The maximum length of the lath martensite, limited by the dendrite arm spacing, was in a range of 15 – 20 μm. Normally, the lath martensite provides a better combination of strength and toughness in tool steels. The short and fine lath martensite along with the refined dendritic microstructure in the laser-clad P20 could further enhance its mechanical properties. Figure 5(d) shows an interface between P20 clad (or more accurately, it should be referred as to dilution zone) and heat affected zone (HAZ), where the clad material shows refined dendrites while the HAZ shows martensitic microstructure. Both zones and the interface between them are indicated by arrows in the above Figure. Figure 5(e) reveals more detail martensitic microstructure in the HAZ.

The metallographic observation on the top surface of as-clad P20 reveals the same morphology as that along the cross-section. It is a refined dendritic microstructure. The majority of phases are lath martensite in combination with a small amount of lower bainite and retained austenite (see Figures 6(a)-(d)). Based on these observations, it is evident that no significant directional solidification was exhibited in the P20 clad, which is also in agreement with the XRD results.

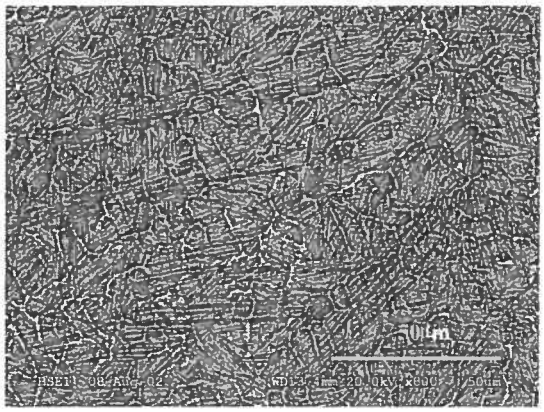

800x

(a) BSE image

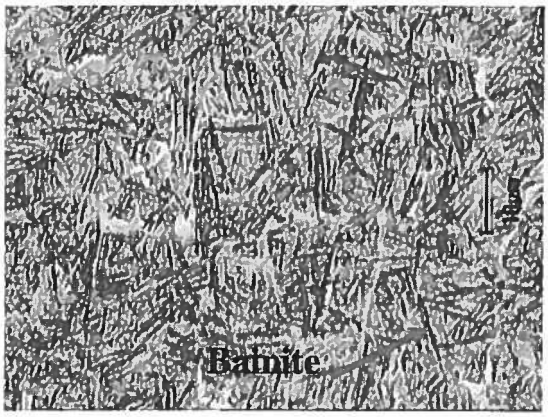

1,000x

(b) Optical photo

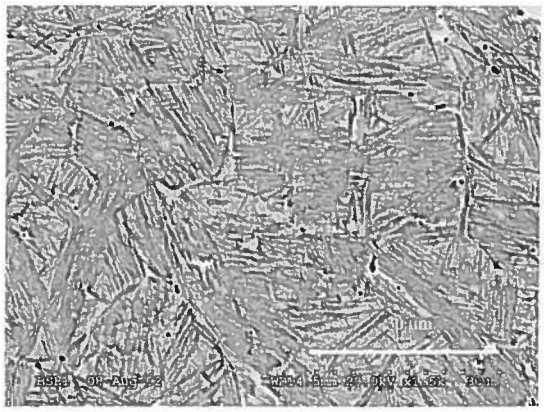

1,500x

(c) BSE image

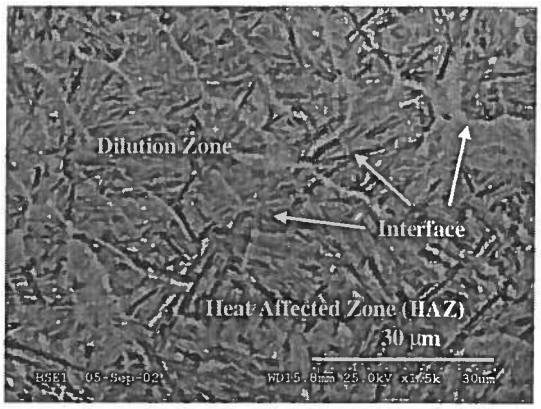

1,500x

(d) BSE image

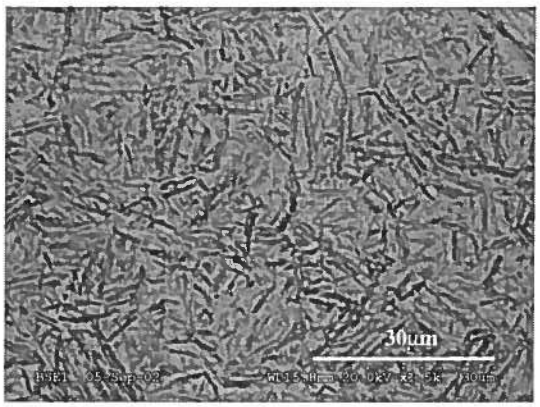

1,500x

(e) BSE Image

Figure 5: Optical and SEM microstructures of as-clad P20 along cross-section

Table 2 lists the X-ray EDS spot analysis results of Si, Cr, Mn, Mo and Fe in the clad layer, dilution zone and substrate. The chemical composition in the dilution zone was very similar to that of the substrate. However, because the P20 powder and the P20 substrate were manufactured by different processes, there was slight difference in their chemical compositions. For example, the Si, Cr and Mo contents were slightly higher in the clad than that in the substrate.

The laser cladding process generated a chemically homogeneous P20 clad layer. As a well-known phenomenon, composition segregation is always associated with dendritic structure in castings. During the solidification prior solidified dendrites always eject solute atoms into the unsolidified liquid at interdendritic regions. This leads to solute-rich interdendritic regions. However, the fast cooling during solidification significantly minimizes the composition segregation. Table 3 lists X-ray EDS spot analysis results, which reveal that interdendritic regions have only slightly higher alloying elements as compared to the intradendritic regions. The X-ray EDS line scans (Figure 7) indicate that, chemical homogenization inside the dendritic microstructure was excellent, and no significant variation in chemical composition was observed under the spatial resolution of the current electron probe. The average chemical composition of the as-clad P20 was almost the same as the P20 powder, indicating that the loss of alloying elements during the laser cladding process was negligible.

In an equilibrium situation, the solidification of liquid P20 steel will start from the formation of a small amount of primary δ (ferrite) dendrites at elevated temperature. Followed by a peritectic reaction, the δ dendrites interact with the solute-rich liquid to form γ (austenite) dendrites. With the further cooling, the γ dendrites grow continuously until all remaining interdendritic liquid transfers to γ phase. At room temperature, the equilibrium microstructure of P20 is a mixture of hypo-eutectoid α (ferrite) and pearlite.

Table 2: The EDS results of P20 clad, dilution zone and substrate (average of 10 spots)

Sample	Si	Cr	Mn	Mo	Fe
P20 clad layer	0.71	2.07	0.49	0.61	96.12
Dilution zone of P20 clad	0.35	1.66	0.80	0.31	96.89
P20 substrate	0.43	1.72	0.96	0.31	96.59

Table 3: The EDS results of P20 powder and as-clad P20 (average of 10 spots)

Sample	Si	Cr	Mn	Mo	Fe
P20 powder	0.63	1.98	0.60	0.55	96.24
Interdendrite of as-clad P20	0.88	2.34	0.71	1.04	95.04
Dendrite of as-clad P20	0.62	1.95	0.67	0.61	96.16

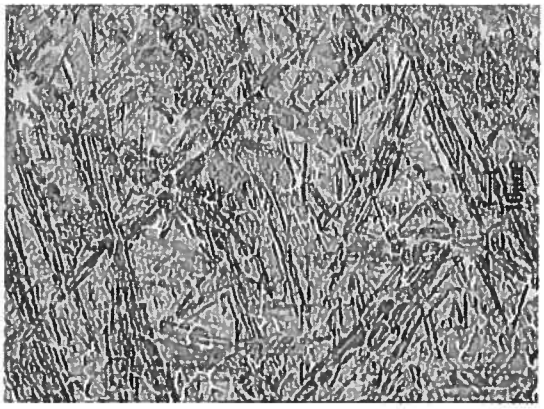

500x

(a) Optical photo

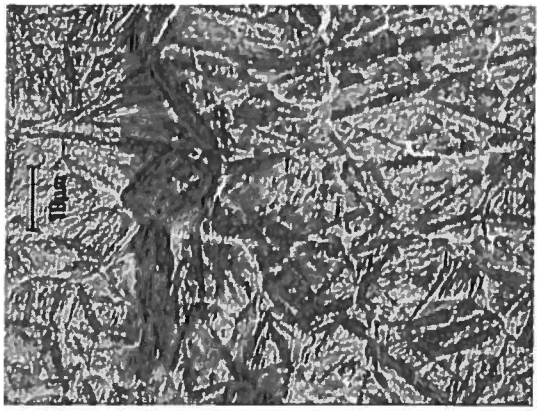

1,000x

(b) Optical photo

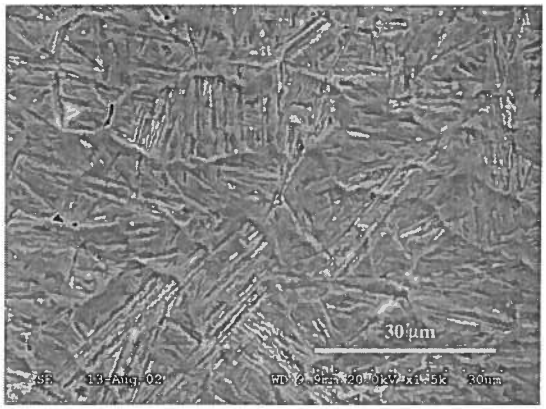

1,500x

(c) SE image

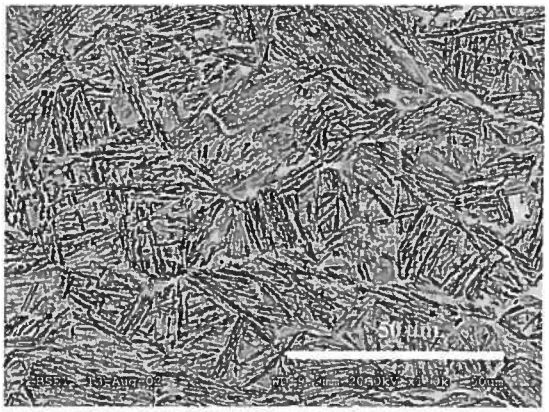

1,000x

(d) BSE image

Figure 6: Optical and SEM microstructures of as-clad P20 on clad surface

However, laser cladding is a faster cooling process that produces non-equilibrium phases. Due to the fast cooling during the solidification, very fine and chemically homogeneous γ dendrites were formed. For the subsequent cooling period, the majority of γ dendrites directly transformed into martensitic phase. However, this cooling rate might not be high enough to completely avoid the bainite nose (referred to P20 tool steel Time-Temperature-Transform (TTT) curve[12]). As an evidence, a small amount of lower bainite was observed. On the other hand, the time to cross the bainite region in the TTT diagram was extremely short, and thus only very small amount of γ dendrites could transform into the lower bainite, while the remaining austenite transformed into martensite plus a little amount of retained austenite. The Transmission Electron Microscope (TEM) study could verify the presence of lower bainite and identify precipitated carbides.

Microhardness of the Clad Layer

Figure 8 shows the variation of microhardness in the P20 clad and the P20 substrate as a function of the distance from the interface. The result indicates that the microhardness of the P20 clad layer reached around 700 HV_{100} (equivalent to Rc. 56-58). The microhardness dropped to 500 HV_{100} near the interface region and heat affected zone (HAZ), and then gradually reduced to about 450 HV_{100} (equivalent to Rc. 48-49) at the substrate.

The high hardness in the clad layer could be attributed to the formation of short and fine lath martensite along with the refined dendritic microstructure. The decrease

in the hardness near the interface region can be attributed to the repeated self-tempering induced by the multiple layer cladding. In other aspects, heat affected zone (HAZ) has slightly higher hardness than the substrate although the substrate was also quenched. This could be attributed to the rapid heating (austenitizing) and rapid cooling (quenching) in the HAZ during the cladding of the first layer. In general, the hardness of the as-clad P20 was higher than that of the heat-treated P20 substrate. As a reference, oil quenched P20 can reach Rc. 36-38[10] while water quenched P20 achieved Rc. 49. Nevertheless, the hardness for both quenched P20 materials was still lower than that of the as-clad P20.

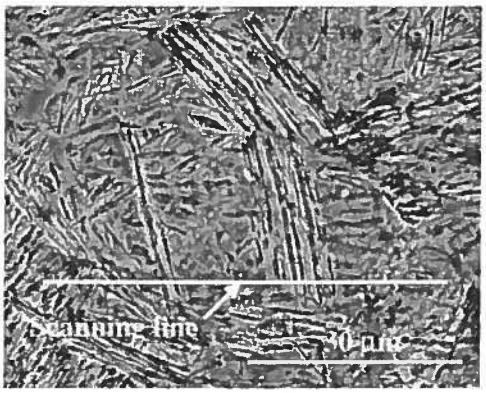

(a) BSE Image

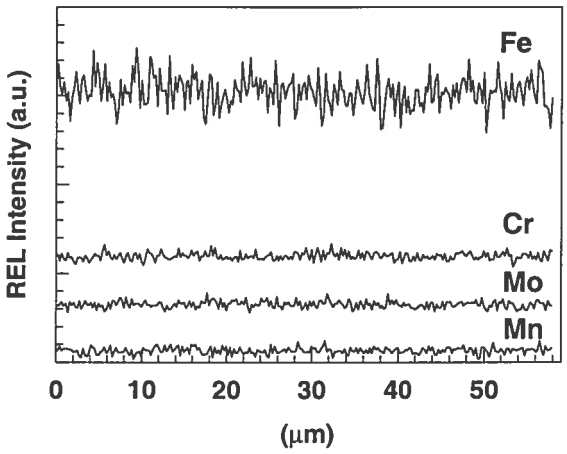

(b) X-ray EDS line scans

Figure 7: The EDS line scans of as-clad P20 for element Cr, Mo, Mn and Fe

Process-induced residual stresses

The process-induced residual stresses were determined using a hole drilling method. During the calculation, the Young's modulus of as-clad P20 was taken as average 210.3 GPa[13]. The measured results represented the average residual stress values across a depth of 0.6 mm from the surface of the clad. Although the actual residual stresses might not be uniform along the depth of the clad layer, these measured values in certain degree reflect the nature and magnitude of the process-induced residual stresses. Table 4 lists the measurement results, which indicates that after the laser cladding, as-clad P20 demonstrated relatively high compressive residual stresses (-137 to - 293 MPa). The residual stress parallel to the laser pass direction was slightly lower than that perpendicular to the laser pass direction. In comparison with the other laser clad materials such as cobalt based Stellite 6 clad on A36 carbon steel[14], laser clad P20 on P20 base material showed residual stresses in compression instead of tension.

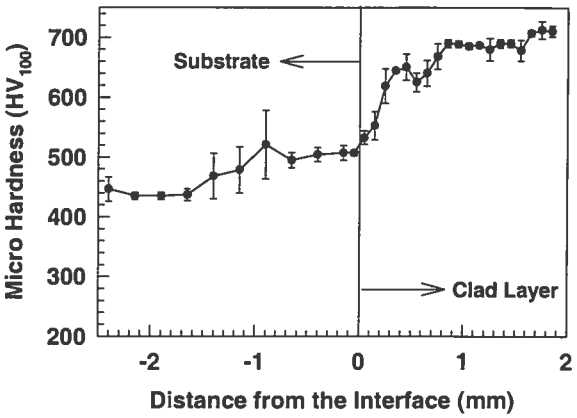

Figure 8: Microhardness profile of laser-clad P20

Normally the residual stresses induced by cladding process are tensile. Because the shrinkage of clad material during the solidification is restricted by the cold substrate, tensile residual stresses are generated in the surface of the clad. If no subsequent solid-state transformation happens, these tensile stresses would remain at the room temperature. However, if any solid-state phase transformation occurs, the final residual stress state would be determined by the volumetric change introduced by the transformation. In this study, laser-clad P20 experienced martensitic transformation in the solid state region. The compressive stresses induced by the volumetric expansion during martensitic transformation may have compensated the tensile stresses caused by the volumetric shrinkage due to the solidification. As a result, the final residual stresses on the surface of the P20 clad were in compression instead of tension. The presence of compressive residual stresses would improve the fatigue properties.

Table 4: Residual stresses of as-clad P20

Sample No.	Parallel to the pass (MPa)	Perpendicular to the pass (MPa)
1#	-225.7	-229.4
2#	-204.3	-292.8
3#	-137.4	-173.6

SUMMARY

(1) The P20 powder material was laser clad on to the AISI P20 tool steel without pre-heating.
(2) The microhardness of as-clad P20 is around HV_{100} 700 (equivalent to Rc. 56-58), which is higher than that of water quenched P20 tool steel (HV_{100} 450, equivalent Rc. 48-49), and much higher than that of oil quenched P20 (Rc. 36-38[10]).
(3) The microstructure of as-clad P20 consists of a majority of lath martensite plus a small amount of lenticular lower bainite and retained austenite. The dendritic microstructure was refined due to fast cooling during the solidification. Thus, a better combination of strength and toughness could be expected.
(4) Laser-clad P20 exhibits uniform chemical composition. No significant segregation was observed.
(5) As-clad P20 demonstrates compressive residual stresses instead of tensile stresses on its surface, which could be beneficial to the improvement of its fatigue properties.

ACKNOWLEDGEMENT

Authors would like to thank Mr. J. Fenner for his important role in the process development, and Mr. M. Botros and Mr. M. Meinert for their contributions in specimen preparation and characterization. A high appreciation also goes to Mr. M.U. Islam, Director of Production Technology Research (PTR-IMTI), for his technical review and critical comments on this paper.

REFERENCE

1. T.A. Jensen, "Surface cladding" in LIA Handbook of Laser Materials Processing, J.F. Ready and D.F. Farson (eds.), pp.284-287, Laser Institute of America/Magnolia Publishing Inc. (2001).
2. W.M. Steen, Laser Material Processing (2nd Ed.), pp.248-251, Springer, London (1998).
3. J.M. Yellup, *"Laser cladding using the powder blowing technique"*, Surface and Coating Technology, 71, 121-128(1995).
4. S. Shah and N.B. Dahotre, *"Microstructural and tribological characterization of laser surface engineered VC coating on tool/die steel"*, Materials and Manufacturing Processes, 17(1), 1-12(2002).
5. W. Guo and A. Kar, *"Microstructural analysis and performance evaluation in laser cladding of stainless steel on the surface of plain steel"* in Elevated Temperature Coatings: Science and Technology III, M. Hampikian and N.B. Dahotre (eds.), pp.231-241, The Minerals, Metals & Materials Society (1999).
6. L. Xue, J.-Y. Chen, C.V. Hyatt and M. Islam, *"Laser cladding with continuous Ni-Al bronze wire feeding for repairing marine components"* in ICALEO' 1999, pp. 58-67, Laser Institute of America (1999).
7. L. Xue, J.-Y. Chen, M.U. Islam, J. Pritchard, D. Manente, and S. Rush, *"Laser consolidation of Ni-based IN-738 superalloy for repair gas turbine blades"* in ICALEO'2000, pp.D30-39, Laser Institute of America (2000).
8. Carpenter Powder Products Inc., *Product Certification for Micro-Melt® P20 Powder*, June (2002).
9. G. Roberts, G. Krauss and R. Kennedy, *Tool Steel (5th Ed.)*, p.292, ASM International, Material Park (1998).
10. G. Roberts, G. Krauss and R. Kennedy, *Tool Steel (5th Ed.)*, p.297, ASM International, Material Park (1998).
11. H.J. Niu and I.T.H. Chang, *"Microstructural evaluation during laser cladding of M2 high-speed steel"*, Metallugical and Materials Transactions A, 31A, 2615-2625(2000).
12. G. Roberts, G. Krauss and R. Kennedy, *Tool Steel (5th Ed.)*, p.299, ASM International, Material Park (1998).
13. Engineering Alloys Digest Inc., *AISI Type P20*, Alloy Digest, January (1982).
14. J.-Y. Chen and L. Xue, *"Effect of stress relief treatment on Stellite 6 clad and substrate"*, Intermediate Report for CAE Vanguard, IMTI-NRC, February (2000).